ELSEVIER

Thermochimica Acta 390 (2002) 21–29

thermochimica acta

www.elsevier.com/locate/tca

Partial pressures of Te_2 and thermodynamic properties of Ga–Te system

Ching-Hua Su*

Microgravity Science and Applications Department, SD46, Science Directorate, NASA/Marshall Space Flight Center, Huntsville, AL 35812, USA

Received 25 October 2001; received in revised form 4 February 2002; accepted 5 February 2002

Abstract

The partial pressures of Te_2 in equilibrium with $Ga_{1-x}Te_x$ samples were measured by optical absorption technique from 723 to 1373 K for compositions, x, between 0.333 and 0.612. To establish the relationship between the partial pressure of Te_2 and the measured optical absorbance, the calibration runs of a pure Te sample were also conducted to determine the Beer's law constants. The partial pressures of Te_2 in equilibrium with the GaTe(s) and Ga_2Te_3(s) compounds, or the so-called three-phase curves, were established. From the partial pressures of Te_2 over the Ga–Te melts, partial molar enthalpy and entropy of mixing for Te were derived and they agree reasonably well with the published data. The activities of Te in the Ga–Te melts were also derived from the measured partial pressures of Te_2. These data agree well with most of the previous results except those determined by Predel et al. [Z. Metallkde. 66 (1975) 268]. The possible reason for the high activity of Te measured by Predel et al. [Z. Metallkde. 66 (1975) 268] for $x < 0.60$ is discussed. Published by Elsevier Science B.V.

Keywords: Partial pressures of Te_2; Activities and partial molar enthalpy of mixing of Te; The Ga–Te system

1. Introduction

The III–VI Ga–Te binary system has shown some interesting properties. Liquid Ga–Te alloys are semiconducting in nature and their electronic properties are similar to those of typical semiconducting solids [1]. The solid Ga chalcogenide compounds, such as GaTe and GaSe, are of special interest because they exhibit strong exciton peaks near the absorption edge at room temperature and have potential applications as non-linear and bistable optical devices. The system is also a part of the I–III–V ternary chalcopyrite semiconductors, such as $AgGaTe_2$, which have been recognized recently as promising nonlinear optical materials for use in high-power tunable solid state infrared laser systems based on the process of second-harmonic generation (SHG) and optical parametric oscillation (OPO) [2]. Thermodynamic and phase diagram study of these III–VI systems is particularly relevant because the study not only provides the thermophysical properties of the liquid semiconductors, but also the required information for the melt crystal growth process.

Over the years, the thermodynamic properties of the Ga–Te system, such as activities, integral and partial molar enthalpy of mixing of the melts and partial pressures over the solid and liquid, have been determined for various compositions, as functions of temperature. Most of the reported data agree reasonably well, except that the activity of Te measured by Predel et al. [3] in the melts at 1114 K is more than 10 times

* Tel.: +1-256-544-7776.
E-mail address: ching.hua.su@msfc.nasa.gov (C.-H. Su).

0040-6031/02/$ – see front matter. Published by Elsevier Science B.V.
PII: S0040-6031(02)00061-8

higher than other data for $x_{Te} < 0.60$. There were also conflicting reports on the Ga–Te phase diagram [4–8].

In this paper, the partial pressures of Te_2 in equilibrium with five Ga–Te samples of different compositions were measured by an optical absorption technique from 723 to 1373 K. To establish the relation between the partial pressure of Te_2 and the measured optical absorbance, a calibration run with pure Te sample was conducted to determine the Beer's law constants. For the first time, the partial pressures of Te_2 in equilibrium with the GaTe(s) and Ga_2Te_3(s) compounds, or the so-called three-phase curves, were established. The activities of Te in the Ga–Te melts were derived from the measured partial pressures of Te_2. These data agree well with most of the previous results and the possible reason for the high activity of Te for $x_{Te} < 0.60$ measured in [3] is discussed.

2. Experimental

The T-shaped optical cells were made of fused silica. The top of the T-shaped cell consisted of a 18 mm o.d. and 15 mm i.d., cylindrical tube with flat, parallel, quartz windows and an optical path of about 10 cm. The bottom of the T-cell was a sidearm attached to the midpoint of the cell-proper. The sidearm was made by joining coaxially a 6 cm long, 12 mm o.d. and 8 mm i.d. tube, and a 10 cm long 18 mm o.d. and 15 mm i.d. tube. The 12 mm o.d. part was attached to the cell-proper and referred to as the stem, and the larger o.d. part of the sidearm is referred to as the reservoir section. A 12 mm o.d. and 8 mm i.d. tube was attached to the reservoir section for vacuum connection during seal-off. A schematic diagram of the optical cell placed in a T-shaped furnace used for the optical measurements is shown in Fig. 1. The volumes of the empty cells were measured as a function of the length along the sidearm by adding distilled water with 0.1 ml resolution. The empty cells were successively rinsed with distilled H_2O, 49 wt.% HF; distilled H_2O, methanol; distilled H_2O, acetone; and distilled H_2O and then dried in a box furnace at about 400 K. The cells were baked at about 1353 K for 18 h under vacuum.

The starting materials are 99.99999% pure Ga from Alfa Aesar, and four times zone refined Te from Johnson Matthey. The amount of sample, the composition and the optical path length for each optical cell are listed in Table 1. The weighed elements were loaded directly into the baked-out optical cells, which were sealed off at a vacuum less than 0.013 Pa after about 30 min of evacuation. The free volume of the cells was then determined from the sealed positions to be about 36 ml.

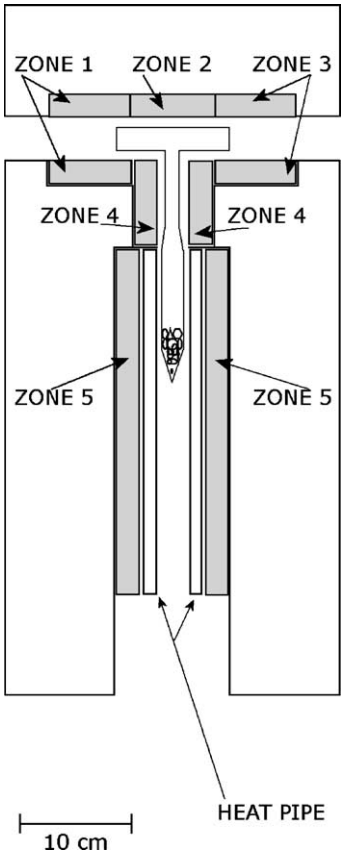

Fig. 1. A schematic diagram of the cross-section of a T-shaped, fused silica optical cell in a five-zone furnace. The top of the furnace (zones 1 to 3) consists of two halves hinged together. The sample beam of the spectrophotometer passes through the top of the T. A ceramic tube liner (not shown) is positioned between furnace bore and the optical cell-proper.

The sealed cells were placed inside a five-zone T-shaped furnace as shown in Fig. 1. The top of the T was approximately 30 cm long and 4 cm i.d. and had three independently controlled heating zones. The two zones on the side (zones 1 and 3) consisted of two 7.5 cm long semi-cylindrical heating elements connected in parallel and the central zone (zone 2) had one

Table 1
Optical cells, total sample weights, sample composition, x in $Ga_{1-x}Te_x$ and optical path length

Cell	Sample weight (g)	x in $Ga_{1-x}Te_x$	Path length (cm)
Te	3.316	1.0	9.90
GaTe-6	3.5830	0.612	9.90
GaTe-7	4.4646	0.489	9.92
GaTe-8	3.5830	0.333	9.90
GaTe-9	3.5695	0.583	9.98
GaTe-10	3.1674	0.520	9.95

7.5 cm long semi-cylindrical element. A ceramic tube liner, 28 cm long (not shown in Fig. 1), is positioned between the furnace bore and the optical cell-proper to block any stray light. The stem and the reservoir sections were heated, respectively, by a 4 cm i.d., 7.5 cm long, and a 6.5 cm i.d., 30 cm long cylindrical element. A 30 cm long, 4 cm i.d., 6 cm o.d. heat pipe furnace liner (Dynatherm Corp.), with Na working fluid inside, was inserted between the furnace bore and the cell reservoir section to improve sample isothermality. Three K-type (Ni–Cr/Ni–Al) thermocouples were positioned along the optical cell-proper and three more K-type thermocouples, calibrated with standards and instrumentation traceable to NIST, were positioned along the stem and the sample section to monitor the temperature along the sample.

The furnace with the optical cell inside was then placed in the path of the sample beam of a double-beam, reversed-optics spectrophotometer (OLIS Inc., model 14H) with the reference beam passed under the furnace. The optical density, defined as $D = \log_{10}(I_{\text{reference}}/I_{\text{sample}})$, where I is the intensity (of reference or sample beam), was measured between the wavelengths of 200 and 700 nm. The light source was a deuterium lamp with wavelengths below 288 nm and a Xenon lamp with wavelengths above 288 nm. The typical instrument band pass was 0.16, 1.1 and 2.7 nm, respectively, at the wavelengths of 600, 288 and 200 nm. The temperature of the optical cell-proper, T_{OC}, was kept at 1323 or 1373 ± 2 K, while the stem and the reservoir sections were maintained at a temperature, T_R, that was the same as or lower than T_{OC}. A baseline spectrum was measured first for each T_{OC} with the reservoir temperature below 670 K.

3. Results and analysis

3.1. Te calibration runs and Beer's law constants

Over the range of temperature and pressure studied here, the Te vapor species is essentially all diatomic [9]. The Beer's law constants for Te_2, defined as $\alpha = Pl/D$, where P is the vapor pressure of Te_2 and l is the optical path length, have been determined for T_{OC} at 1028 [10], 1073, 1133 [11] and 1273 K [12]. For this study, the Beer's law constants at 1323 and 1373 K are needed. The measured optical density spectrum for the pure Te cell with T_{OC} at 1323 K and T_R at 876.5 K is plotted in Fig. 2. It shows a vibronic spectrum in the wavelength region between 300 and 600 nm, which is consistent with the published absorption spectra of Te_2 [10–12]. The measured optical density was noisy at low wavelength region, where the measurable upper limit for D was 3.5 to 4, because the sample beam intensity has reduced to the same order of magnitude as the dark current in the photomultiplier tube detector.

From a recent third law analysis of the vapor–liquid–solid equilibrium for Te [13] the vapor pressure of Te_2 above the melting point of Te can be expressed by four different equations for four-temperature ranges between 723 and 1750 K. Since most of our P_{Te_2} data were in the range of 100–30,000 Pa, the expression given for the temperature range of 922–1143 K

$$\ln P^0_{Te_2} = \frac{-13,724}{T} + 22.392 \quad (1)$$

was used for the whole temperature range. The associated errors of P_{Te_2} with this assumption are 15% at P_{Te_2} of 26 Pa, 6% at 178 Pa, and 0% from 1792 to 32,211 Pa.

The net optical density, D, for a set of wavelengths between 420 and 600 nm were plotted against $1000/T_R$, where T_R is the reservoir temperature in K. For both $T_{O.C.}$ (1323 and 1373 K), the data points for each wavelength are parallel to $P^0_{Te_2}$; implying that the absorption of these wavelengths was originated from the same vapor species, Te_2. Using Eq. (1), the Beer's law constants were determined for these wavelengths at both 1323 and 1373 K, and are listed in Table 2. The Beer's law constants determined here are in line with the previous results. For comparison, the Beer's law

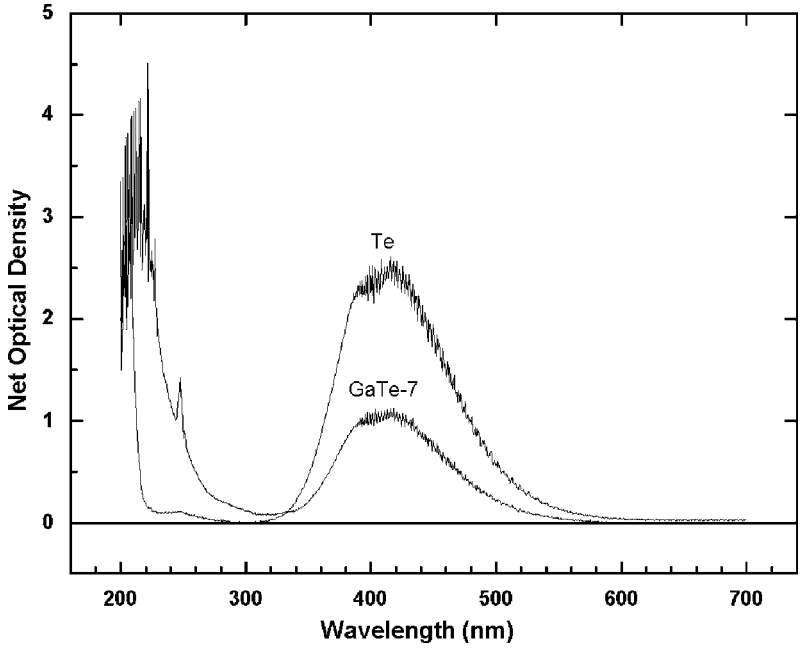

Fig. 2. Optical absorption spectra of the Te and GaTe-7 cells. The reservoir temperatures were 876.5 and 1260.5 K, respectively, for Te and GaTe-7 ($T_{OC} = 1323$ K).

constants determined at 1028, 1133 and 1273 K in [12] are, respectively, 2705, 3009 and 3557 Pa cm for the wavelength of 436 nm and are, respectively, 10,030, 10,340 and 10,440 Pa cm for the wavelength of 490 nm. The main errors in the Beer's law constants can be attributed to the measured errors in D and the reservoir temperature, which were estimated to be less than ± 0.001 and ± 1.0 K, respectively.

Table 2
Beer's law constants, α, in 10^3 Pa cm for Te_2 vapor species

Wavelength (nm)	α at 1323 K	α at 1373 K
422	3.658	3.931
436	4.023	4.266
459	5.573	5.745
473	7.995	7.974
482	9.687	10.10
490	10.44	11.04
500	14.19	14.79
525	28.17	28.37
550	62.92	65.76
575	121.2	139.6
600	250.3	323.9

3.2. Partial pressures of Te_2

The optical absorption spectra of Te_2 were monitored during the initial heat-up of the samples. Except for the $x_{Te} = 0.612$ sample, the observed partial pressures of Te_2 followed that of pure Te at low-temperature region and then, at the temperature range between 1013 and 1043 K, the observed P_{Te_2} dropped by orders of magnitude and reached an equilibrium state within 30 min. For $x = 0.612$, the reaction occurred below the lowest temperature of our measurements at 719 K. After this synthesis reaction, the absorption spectrum was taken after the sample has been at each temperature setting for about 30 min. For two cells, data were also taken the next day with samples at elevated temperatures overnight for 16 h and the observed spectra were consistent with those taken from the previous day.

A spectrum of the GaTe-7 sample with T_{OC} at 1323 K and T_R at 1260.5 K is also plotted in Fig. 2. Beside the vibronic absorption peaks of Te_2 the spectrum shows additional absorption features between 200 and 300 nm. Similar absorption feature was observed

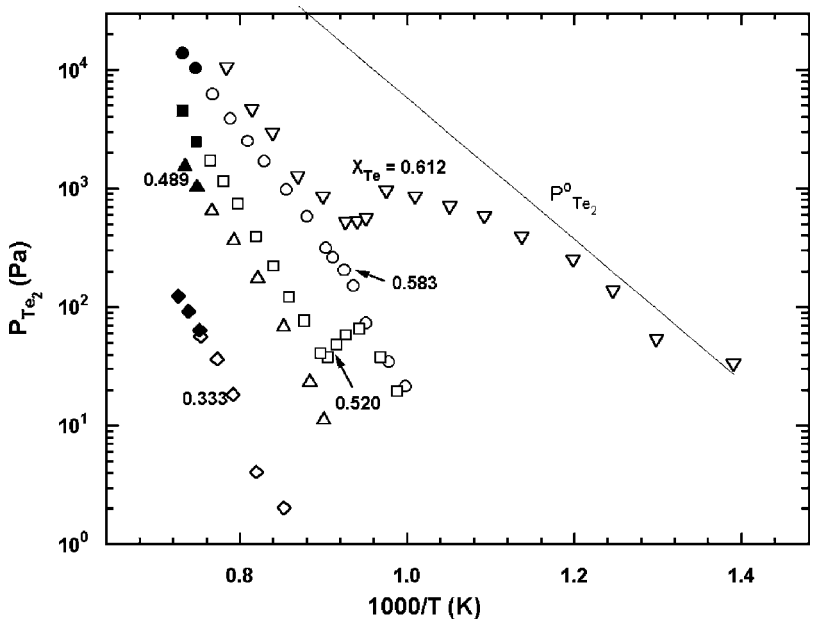

Fig. 3. The measured values of $\log_{10} P_{Te_2}$ (Pa) plot against $1000/T$ (K) for pure Te and GaTe samples of various compositions. The open and closed symbols are for, respectively, optical cell temperatures of 1323 and 1373 K.

for all of the GaTe samples. From the results of mass spectroscopy measurements [14,15], Ga_2Te was determined to be the other predominant vapor species besides Te_2. Therefore, this absorption band is believed to be associated with the Ga_2Te vapor species.

Using the Beer's law constants given in Table 2, the partial pressures of Te_2 were determined from the measured D for the GaTe samples as a function of temperature. The pressure value was taken as the average of, typically, four to eight wavelengths, and is plotted, together with the pressure of Te_2 over pure Te, as a function of $1000/T$ in Fig. 3. The measured pressures ranged from 2 to 2×10^4 Pa and the results from two optical cell temperatures, 1323 and 1373 K, agree well.

The partial pressures of Te_2 over $x_{Te} = 0.612$ show a segment of Ga_2Te_3(s) three-phase curve at the low-temperature range, i.e. the partial pressures in equilibrium with the Te-saturated Ga_2Te_3(s), and after going through a maximum and a minimum the curve, breaks off into the liquid phase. The liquidus temperature for $x_{Te} = 0.612$ is estimated from the break point to be between 1063 and 1079 K, which is consistent with the published melting point of 1071 ± 10 K [16] for Ga_2Te_3(s).

The P_{Te_2} data over $x_{Te} = 0.583$ have three data points at the low-temperature region and can be expressed as:

$$\ln P_{Te_2} = \frac{-26,011}{T} + 29.026 \quad (2)$$

These three data are believed to be the partial pressures in equilibrium with the Te-saturated Ga_3Te_4(s) and Ga-saturated Ga_2Te_3(s). The next data point at higher temperature is believed to be on the three-phase curve of the Ga-saturated $Ga_2Te_3(s)$ + liquid. The rest of the data break off from the three-phase curve into the $x_{Te} = 0.583$ melt. The liquidus for $x_{Te} = 0.583$ is estimated to be between 1068 and 1081 K.

For the $x_{Te} = 0.520$ sample, the three data in the low-temperature region represent the three-phase curve of the Te-saturated GaTe(s) and Ga-saturated Ga_3Te_4(s). They can be represented by:

$$\ln P_{Te_2} = \frac{-26,339}{T} + 29.057 \quad (3)$$

The rest of the data go through a maximum and a minimum and then break off between 1104 and 1115 K, in agreement with the published liquidus temperature for $x_{Te} = 0.520$ [16,17].

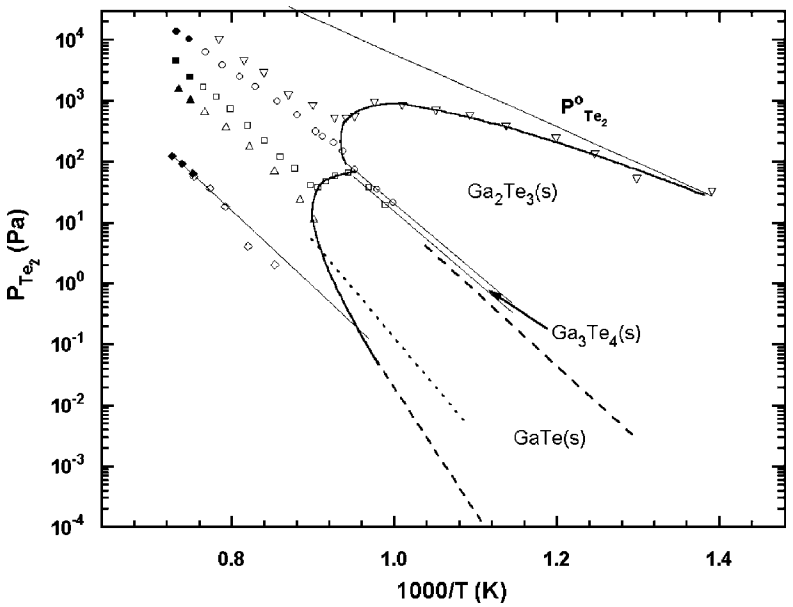

Fig. 4. A similar plot as Fig. 3 including our data and previously published results. The three-phase curves for Ga_2Te_3(s), Ga_3Te_4(s) and GaTe(s) are shown as the solid curves. The P_{Te_2} data from [15] for Te- and Ga-saturated GaTe(s) are shown as dashed lines and the data from [18] for $x_{Te} = 0.49$ are shown as dotted line.

The liquidus temperatures reported for the other two samples, $x_{Te} = 0.489$ and 0.333 were about 1105 ± 2 and 1023 ± 5 K [16,17], respectively. Our P_{Te_2} data for these two samples are believed to be in the liquid phase, except maybe the lowest point for $x_{Te} = 0.489$ which was at the Ga-saturated three-phase curve of GaTe(s). For $x_{Te} = 0.333$ the deviation of the two lowest data from a straight line is believed to be due to the large error associated with the measurements of P_{Te_2} at the low-pressure range.

The partial pressures of Te_2 over GaTe(s) have been measured previously, mainly in the low-pressure range, by Plotnikov et al. [15], and Mukdeeprom-Burckel and Edwards [18], using mass spectroscopy and effusion method, respectively. The P_{Te_2} measured here are plotted in Fig. 4 with the previous results. The difference of about a factor of two in our data for $x_{Te} = 0.583$ and 0.520 in the low-temperature region implies the existence of the intermediate phase Ga_3Te_4(s). The three-phase curves for Ga_2Te_3(s), Ga_3Te_4(s) and GaTe(s) established from our data are connected by the solid curves. The P_{Te_2} data for the Te-saturated GaTe(s) from [15] agree reasonably well with our results and their results in the low-pressure range for the Ga-saturated GaTe(s) are in line with our data in the high-pressure range. The extrapolation of our data for the $x_{Te} = 0.333$ melt to the low-temperature range intercepts the Ga-saturated GaTe(s) curve at about 1028 K, which is also consistent with the liquidus temperature of about 1023 ± 5 K for $x_{Te} = 0.333$ [16,17]. The P_{Te_2} data from [18] for $x_{Te} = 0.49$, shown as dotted line, presumably to be the Ga-saturated GaTe(s), are about one order of magnitude too high.

Since the pressures are usually averaged from 4 to 6 wavelengths, the errors of these values cannot be estimated systematically. In general, the errors in the lower pressure range are high because the data were calculated from 3 or 4 wavelengths with small values of D and because of the large error associated with using Eq. (1). The total error was estimated to be less than 25% for pressure less than 10 Pa and less than 5% for pressure higher than 1×10^3 Pa.

The compositions, as listed in Table 1, are calculated from the amounts of pure elements loaded into the optical cells. During the partial pressure measurements at high-temperatures the samples sublimed into the vapor phase and the compositions of the condensed phase changed form their initial values. In the worst case, assuming that Te_2 is the only vapor species, at the

highest pressure of 1.38×10^4 Pa at 1368 K for the GaTe-7 sample, the composition, x_{Te}, of the condensed phase changed from the initial value of 0.583 to 0.582, assuming ideal gas law for the vapor phase.

3.3. Thermodynamic properties of the Ga–Te melts

The partial pressures of Te_2 in the Ga–Te melts can be fit well by the following expressions:

$$\ln P_{Te_2} = \frac{-a}{T} + b \tag{4}$$

where a and b are constants. The partial molar enthalpy and entropy of mixing for Te, $\bar{H}_{Te}$ and $\bar{S}_{Te}$ in the Ga–Te melts relative to Te(l) can be derived as

$$\mu_{Te} - \mu^0_{Te} = \tfrac{1}{2}RT(\ln P_{Te_2} - \ln P^0_{Te_2}) = \bar{H}_{Te} - T\bar{S}_{Te} \tag{5}$$

and the excess partial molar entropy, $\bar{S}^X_{Te}$, is given by

$$\bar{S}^X_{Te} = \bar{S}_{Te} + R \ln x_{Te} \tag{6}$$

Table 3
The constants a and b in Eq. (4), the partial molar enthalpy, $\bar{H}_{Te}$, and excess partial molar entropy, $\bar{S}^X_{Te}$ of mixing relative to Te(l) in $Ga_{1-x}Te_x$ melts

x_{Te}	a	b	$\bar{H}_{Te}$ (kJ/mol)	$\bar{S}^X_{Te}$ (J/mol K)
0.333	28675	14.163	−62.149	−22.922
0.489	27279	15.895	−56.346	−26.835
0.520	27055	16.585	−55.414	−29.210
0.583	21900	14.048	−33.987	−17.711
0.612	21007	14.094	−30.274	−17.525

Table 4
Te activity, relative to Te(l), a_{Te}, in the melts at 1108 and 1373 K derived from the measured partial pressure of Te_2

x_{Te}	a_{Te} at 1108 K	a_{Te} at 1373 K
0.333	0.00611	0.0225
0.489	0.02726	0.0225
0.520	0.04259	0.1360
0.583	0.1226	0.2499
0.612	0.1877	0.3540

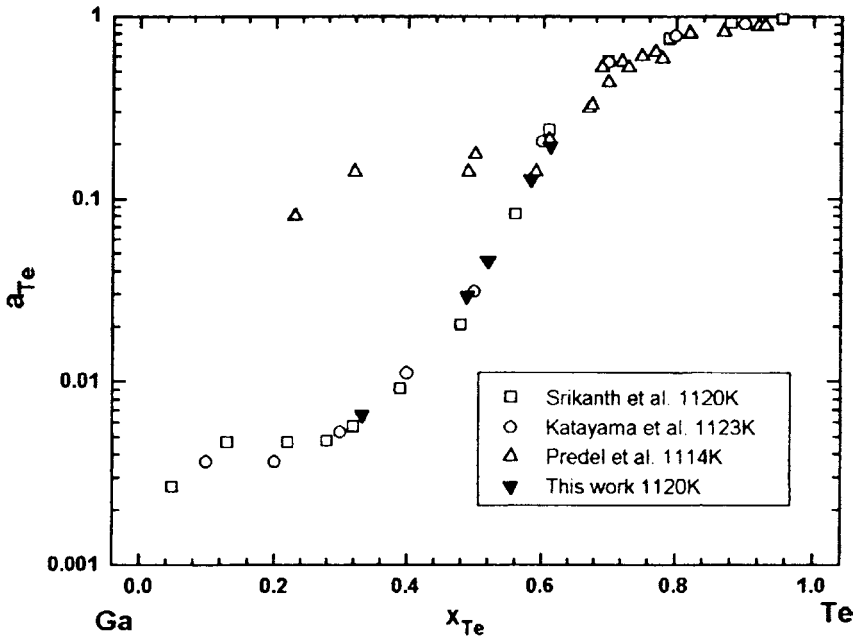

Fig. 5. Te activity relative to Te(l), a_{Te}, as a function of x_{Te}. The results from this study at 1120 K are compared with literature values [3,19,20] between the temperature range of 1114 and 1123 K.

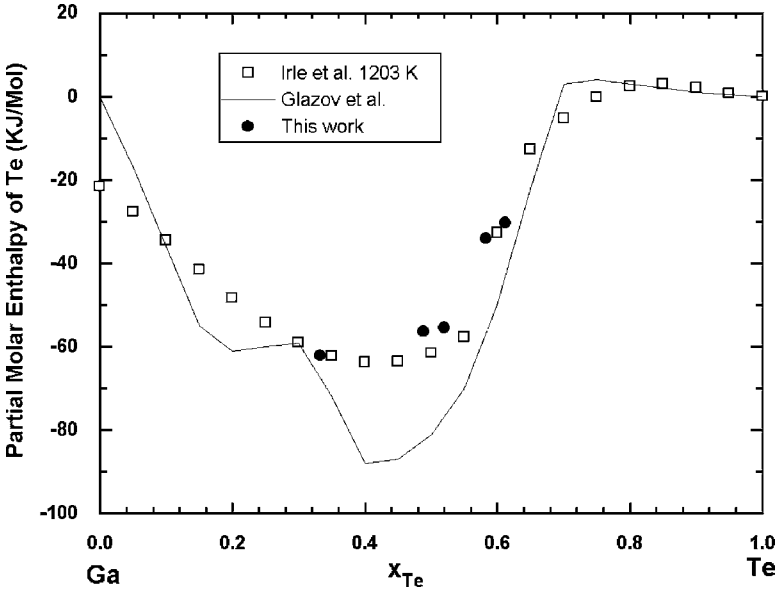

Fig. 6. Partial molar enthalpy of mixing for Te(l) plot against x_{Te}.

where R is the gas constant. The linear fits given by Eq. (4) imply that the derived partial molar quantities, as given in Table 3, are independent of temperature.

The activity of Te in the liquid phase can be derived from

$$a_{Te} = \left(\frac{P_{Te_2}}{P^0_{Te_2}}\right)^{1/2} \tag{7}$$

with $P^0_{Te_2}$ given by Eq. (1). The Te activity at 1108 K, the melting point at GaTe(s), and at 1373 K were calculated, using the constants in Table 3, for these samples and are listed in Table 4. The Te activities, a_{Te}, have been measured by Predel et al. at 1114 K [3], Srikanth and Jacob at 1120 K [19], and Katayama et al. at 1123 K [20]. Fig. 5 shows a_{Te} versus x_{Te} from these results, including ours at 1120 K for comparison. Most of the results agree well, except that the data from Predel et al. [3] for x_{Te} less than 0.6 are an order of magnitude higher than other data. The experimental results of a_{Te} at the melting point of GaTe, as given in Fig. 1 of [21] by Glazov et al., could not be scaled with good accuracy, but the curve generally agrees with the results in Fig. 5 except those data from [3] at low values of x_{Te}.

The data of partial molar enthalpy of mixing for Te, together with the published results, are plotted in Fig. 6. Our data agree well with those determined from heat-flow calorimetry by Irle et al. [22]. The data determined by Glazov et al. [21] show several inflection points and a value of 0 kJ/mol at $x_{Te} = 0$. These data are considered to be less reliable because they were obtained using a curve fitting and smoothing algorithm from the e.m.f. measurements and the subsequent Gibbs–Duhem integration.

The errors in the partial molar enthalpy and entropy of Te determined here are difficult to assess. The errors came from the uncertainty in the measured P_{Te_2}, which are estimated to be in the 5–10% range, and the standard deviation in the linear fitting to Eq. (4). In general, the errors associated with $\bar{H}_{Te}$ and $\bar{S}_{Te}$ are estimated to be less than 5%.

4. Discussions

The activity of Te data measured by Predel et al. [3] shown in Fig. 5 was derived from the measured P_{Te_2}. In their experiments [23], pure Ga and Te elements were loaded into a sealed evacuated ampoule and were positioned at two ends with the Ga sample at

a temperature about 25–350 K higher than that of Te. With the addition of Te to the Ga sample through vapor transport, the Ga sample eventually became $Ga_{1-x}Te_x$ when the system reached equilibrium. After cool-down, the composition x_{Te} was determined from the sample weight of the GaTe sample, assuming that the weight change was solely caused by the addition of Te. The partial pressure of Te_2 was determined from the Te sample temperature assuming that it was pure Te. These assumptions would be valid if the only vapor species in the system is Te_2. However, as discussed earlier, from the previous mass spectroscopy experiments that, beside Te_2, Ga_2Te is also a predominant vapor species. Therefore, under the experimental condition in [3,23] there was another vapor flux of Ga_2Te from the Ga to the Te sample when the Ga sample was incorporated with Te. In this case, the two assumptions were not valid because (1) the weight change in the GaTe sample can not be solely attributed to the addition of Te, and (2) with the addition of Ga from the Ga_2Te vapor flux, the Te sample was no longer pure Te. The worst situation was for samples with low x_{Te} because these samples are supposed to have high partial pressure of Ga_2Te. Fig. 5 shows that the Te activity data from Predel et al. [3] for x_{Te} less than 0.6 are one order of magnitude higher than other data. Firstly, the real Te content in these $Ga_{1-x}Te_x$ sample maybe higher than what they reported due to the loss of Ga from the sample and secondly, the real partial pressure of Te_2 may be lower than what they reported because the pure Te reservoir was contaminated with Ga.

Acknowledgements

The author would like to thank G. Nelson of University of Alabama in Huntsville for making the optical cells. This work was supported by the Office of Biological and Physical Research of the National Aeronautics and Space Administration.

References

[1] M. Cutler, Liquid Semiconductors, Academic Press, New York, 1977.
[2] Materials Research Society Bulletin, 23 (1998) 23.
[3] B. Predel, J. Piehl, M.J. Pool, Z. Metallkde. 66 (1975) 268.
[4] V.W. Klemm, H.U.V. Vogel, Z. Anorg. Allg. Chem. 219 (1934) 45.
[5] P.C. Newman, J.C. Brice, H.C. Wright, Philips Res. Rep. 16 (1961) 41.
[6] H.-U. Tschirner, B. Garlipp, R. Rentzsch, Z. Metallkde. 77 (1986) 811.
[7] R. Blachnik, E. Irle, J. Less-common Met. 113 (1985) L1.
[8] F. Alapini, J. Flahaut, M. Guittard, S. Jaulmes, M. Julien-Pouzol, J. Solid State Chem. 28 (1979) 309.
[9] A. Neubert, High Temp. Sci. 10 (1978) 261.
[10] J.P. Schwartz, T. Tung, R.F. Brebrick, J. Electrochem. Soc. 128 (1981) 438.
[11] C.-H. Su, P.-K. Liao, R.F. Brebrick, J. Electrochem. Soc. 132 (1985) 942.
[12] Y. Huang, R.F. Brebrick, J. Electrochem. Soc. 135 (1988) 486.
[13] R.F. Brebrick, High Temp. Sci. 25 (1988) 187.
[14] O.M. Uy, D.W. Muenow, P.J. Ficalora, J.L. Margrave, Trans. Faraday Soc. 64 (1968) 2998.
[15] M.V. Plotnikov, E.A. Aleshina, A.V. Makarov, V.P. Zlomanov, Izv. Akad. Nauk SSSR, Neorgan. Mater. 19 (1983) 1294.
[16] T.B. Massalski (Ed.), Binary Alloy Phase Diagrams, 2nd Edition, p. 1864, ASM International, 1990.
[17] C.-S. Oh, D.N. Lee, CALPHAD 16 (1992) 317.
[18] P. Mukdeeprom-Burckel, J.G. Edwards, Thermochim. Acta 213 (1993) 47.
[19] S. Srikanth, K.T. Jacob, Thermochim. Acta 153 (1989) 27.
[20] I. Katayama, J.-I. Nakayama, T. Nakai, Z. Kozuka, Trans. Jpn. Inst. Metals 28 (1987) 129.
[21] V.M. Glazov, L.M. Pavlova, A.L. Lomov, E.B. Il'ina, Russ. J. Phys. Chem. 62 (1988) 462.
[22] E. Irle, B. Gather, R. Blachnik, U. Kattner, H.L. Lukas, G. Petzow, Z. Metallkde. 78 (1987) 535.
[23] B. Predel, J. Piehl, Z. Metallkde. 66 (1975) 33.